An ab Initio/Rice−Ramsperger−Kassel−Marcus Study of the Reactions of Propenols with OH. Mechanism and Kinetics of H Abstraction Channels

Chong-Wen Zhou,[†,‡] Alexander M. Mebel,[*,‡] and Xiang-Yuan Li[*,†]

College of Chemical Engineering, Sichuan University, Chengdu, 610065, People's Republic of China, and Department of Chemistry and Biochemistry, Florida International University, Miami, Florida 33199

Received: April 3, 2009; Revised Manuscript Received: August 24, 2009

Propenols have been found to be common intermediates in the hydrocarbon combustion and they are present in substantial concentrations in a wide range of flames. However, the kinetics properties of these species in combustion flames have not received much attention. In this work, the mechanism and kinetics of the OH hydrogen abstraction from propenols are investigated. Three stable conformations of propenols, (*E*)-1-propenol, (*Z*)-1-propenol, and *syn*-propen-2-ol, are taken into consideration. The potential energy profiles for the three reaction systems have been first investigated by the CCSD(T) method. The geometric parameters and relative energies of the reactants, reactant complexes, transition states, product complexes, and products have been investigated theoretically. The rate constants are calculated in the temperature range of 200−3000 K by the Variflex code based on the weak collision master equation/microcanonical variational RRKM theory. For all considered reactions, our results support a stepwise mechanism involving the formation of a reactant complex in the entrance channel and a product complex in the exit channel. In the reaction of OH with (*E*)-1-propenol, the hydrogen abstractions from the $-CH_3$ and $-OH$ sites are dominant and competitive with each other in the temperature range from 500 to 2000 K. Above 2000 K, the hydrogen abstraction from the $-CH$ group bonded to O atom becomes dominant with a relative yield of 51.1% at 3000 K. In the reaction of OH with (*Z*)-1-propenol, the hydrogen abstractions from $-CH_3$, $-CH$ bonded to O atom, and $-OH$ are preferable in the temperature range from 500 to 1800 K, with the first two channels being competitive with each other. Above 1800 K, the hydrogen abstraction reaction from the CH group bonded to the CH_3 group becomes dominant with the branching ratio of 90.3% at 3000 K. In the reaction of OH with *syn*-propen-2-ol, the abstractions from the $-CH_3$ and $-OH$ sites are competitive with each other when the temperature is higher than 500 K, and they become dominant above 800 K with the relative yields of 70.5% and 29.5% at 3000 K, respectively. The predicted total rate constants at the pressure of 1 atm fitted by modified three-parameter Arrhenius expressions in two different temperature ranges are also provided.

1. Introduction

Enols, an entire class of molecules absent from standard hydrocarbon oxidation models in the past over 150 years, have been recently observed in a wide range of hydrocarbon flames by Taatjes et al.[1] The enols were first postulated by Erlenmeyer[2] in 1880 as transient chemical intermediates, but the simplest enol, ethenol (vinyl alcohol, CH_2═CHOH), was not directly identified until 1973[3] and not observed in the gas phase until 1976.[4] In the traditional hydrocarbon combustion chemistry, they are all treated as the aldehydes or ketones. However, recent experimental results[1,5,6] show that the enols such as ethenol, propenols, and butenols are common intermediates in the hydrocarbon combustion and they are present in substantial concentrations in a wide range of flames.

The experiments carried out by Taatjes et al.[1] demonstrated that propen-1-ol and propen-2-ol also occur in hydrocarbon flames. Mole fraction profile of propenols from a rich propene flame was measured.[6] Qi et al.[7] investigated the formation of enols in laboratory low-pressure cold plasma discharges in alcohols by employing the single-photon vacuum ultraviolet (VUV) photoionization mass spectrometry, and the identification of propenols in their study strongly suggests that these molecules are potential interstellar species, which may exist in the hot core environments. Hence, understanding of the formation and removal reactions of enols in combustion and interstellar chemistry is necessary. We have theoretically investigated the formation mechanism of propenols and ethenol in rich propene flame through the reaction of OH with propene[8] and the unimolecular decomposition reaction of propen-2-ol and the related H + CH_2COHCH_2 reaction in combustion conditions.[9] Rate constants for each reaction channel and the product branching ratios have also been studied. But this is not sufficient for understanding the propenols chemistry in flames; detailed theoretical analyses of their removal reactions with flame radicals, such as OH and H, are still unavailable. In this work, we report a study of the reactions of enols, here propenols, with OH over a wide range of combustion conditions. Theoretical characterization of these reactions would be helpful for elucidating the chemistry of enols in flames.

In the present study, each hydrogen abstraction path of the OH + propenols reactions has been considered as a complex mechanism involving the formation of a reactant complex in the entrance channel and a product complex in the exit channel. According to recent theoretical studies,[10−15] a prereactive complex has been identified in the reactions of oxygenated and unsaturated compounds with OH radical. Alvarez-Idaboy et al.[11]

* Authors to whom correspondence should be addressed: mebela@fiu.edu (A.M.M.) and xyli@scu.edu.cn (X.-Y.L.).
† Sichuan University.
‡ Florida International University.

10.1021/jp903103s CCC: $40.75
Published on Web 09/11/2009

concluded that prereactive complexes seem to be common in all radical−molecule reactions, and they are due mainly to the long-range Coulomb interactions between the reactant molecules. Galano[15] studied the reaction of OH with hydroxyacetone in detail and found reactant complexes in every entrance channel and product complexes in every exit channel. Smith et al.[16] reviewed the role of these intermediates in bimolecular reactions. Loomis et al.[17] and Lester et al.[18] studied reactant complexes involving the OH radical experimentally. Moreover, it has been established that the presence of an attractive well in the entrance channel of a potential energy surface can influence the dynamics and, hence, the course of the reaction.[16] It is proposed that if the reaction occurs at pressures high enough for these complexes to be collisionally stabilized and if the energy barriers are small, they are likely to play an important role.[11] Sekušak and Sabljić[19] have also found that such intermediate complexes play a key role in hydrogen abstraction reactions from haloethanes. The existence of a reactant complex can manifest itself in terms of negative temperature dependence of the reaction rate constant, which is expected when there is an attractive encounter between reactants.

The objective of this work is to provide a comprehensive theoretical treatment of the mechanisms and kinetics for the gas-phase hydrogen abstraction reactions of OH with propenols, which are expected to be important pathways of the propenols removal in the combustion conditions. Detailed mapping of the potential energy profiles of the reactions will be performed at a high level of ab initio calculations. In addition, rate constants and product branching ratios for each reaction will also be studied and the results will be extrapolated for high temperature combustion modeling applications. To simplify the analysis of each reaction system, we assumed that once a specific pathway started, it proceeds to completion, independently of other pathways, i.e., there is no mixing or crossover between different pathways. On this basis, the overall rate constant (k) that measures the rate of OH disappearance can be determined by summing up the rate constants calculated for each channel.[20] Very little experimental and computational data are available on these reaction channels in neutral gas phase combustion chemistry.

2. Computational Methods

A. Potential Energy Surface Calculations. The BHandHLYP hybrid density functional[21] with the 6-311++G(d,p) basis set has been used to optimize the geometries of all the species including the reactants, transition states, and products. This functional was chosen on the basis of its proven effectiveness.[22−28] Restricted calculations were used for closed shell systems and unrestricted ones for open shell systems. Vibrational frequencies of all species have also been calculated at the corresponding level of theory. All stationary points were identified for local minima (number of imaginary frequencies NIMAG=0) and transition states (NIMAG=1). The intrinsic reaction coordinate[29] (IRC) calculations were carried out to validate the connections between transition states and local minima. To achieve more reliable energies of various species along the PES, we have employed the CCSD(T)/6-311++G(d,p) method to obtain single point energies based on the optimized geometries, and zero point energies (ZPE) corrections were included in all relative energies. All quantum chemistry calculations were carried out using the Gaussion 03[30] and MOLPRO 2006[31] program packages.

B. Rate Constant Calculations. The rate constants for the key reaction steps have been computed with variational transition-state theory (VTST) and Rice−Ramsperger−Kassel−Marcus (RRKM) theory using the Variflex code.[32] The energetic and molecular parameters (reaction barriers, rotational constants, vibrational frequencies) from the ab initio calculations were used in this rate constant calculation. The component rates were evaluated at the E, J-resolved level. The pressure dependence of rate constants was treated by one-dimensional (1D) master equation calculations using the Boltzmann probability of the complex for the J distribution. The master equation was solved by eigenvalue-solver based approach for the dissociation processes.[33,34] In order to achieve convergence in the integration over the energy range, an energy grain size of 100 cm^{-1} was used. The total angular momentum J covered the range from 1 to 241 in steps of 10 for the E,J-resolved calculation. Reactions with tight transition states were treated using a canonical nonvariational transition state theory.[35] It should be noted that the RRKM calculations would have two possible sources of error. First, the method of ab initio calculations applied here is able to provide accuracy in relative energies in the range of 1−3 kcal/mol, which is sometimes comparable with binding energies of weak hydrogen-bonded complexes we encounter in the present work. Second, the RRKM method may not be accurate when the potential energy wells of the decomposing intermediates are shallow, because the intramolecular vibrational redistribution (IVR) may not be fast enough to warrant the use of the statistical theory. Nevertheless, we used a similar ab initio/RRKM approach earlier for the reaction of OH with propene[8] and found a good agreement of the calculated rate constants with experiment. The RRKM approach has also been used to deal with the processes with shallow wells in the studies of the OH + C_2H_4[36] and CH_3 + C_2H_5[37] reactions and the predicted RRKM rate constants agreed well with the experimental values.

3. Results and Disscussion

A. Potential Energy Profiles and Reaction Mechanisms. As alluded to in section 1, we shall consider the hydrogen abstraction channels for the reactions of propenols with OH. 1-Propenol has three internal rotational degrees of freedom, the CH_3−CH, CH−CH, and CH−OH bond torsions. Several different minima were fully optimized at the BHandHLYP/6-311++G(d,p) level and two most stable conformations, (E)-1-propenol and (Z)-1-propenol, will be taken into consideration in this work. Propen-2-ol also has different isomers, but here we consider only the most stable form of *syn*-propen-2-ol, which has been proved[9] to be the preferred form of propen-2-ol in the gas phase.

All possible reaction sites for hydrogen abstraction in these three species are investigated. The reaction channels for 1-propenols can be written as shown in eqs 1−4.

$$CH_3CHCHOH + OH \rightarrow CH_2CHCHOH + H_2O \quad (1)$$

$$\rightarrow CH_3CCHOH + H_2O \quad (2)$$

$$\rightarrow CH_3CHCOH + H_2O \quad (3)$$

$$\rightarrow CH_3CHCHO + H_2O \quad (4)$$

The reaction channels for *syn*-propen-2-ol can be described as shown in eqs 1a−3a.

Each of these reactions has three steps. First, a reactant complex (**RC**) is formed through barrierless recombination of the reactants in the entrance channel; second, the product complex (**PC**) is formed by H abstraction in **RC** through a

$$CH_3COHCH_2 + OH \rightarrow CH_2COHCH_2 + H_2O \quad (1a)$$

$$\rightarrow CH_3COHCH + H_2O \quad (2a)$$

$$\rightarrow CH_3COCH_2 + H_2O \quad (3a)$$

corresponding transition state; and finally, the products (a radical and water) are formed from the corresponding **PC** in the exit channel.

The geometry optimizations of the reactants, reactant complexes (**RC**s), transition states, product complexes (**PCs**), and products for the reactions of OH + (*E*)-1-propenol, OH + (*Z*)-1-propenol, and OH + *syn*-propen-2-ol, have been carried out. The cooresponding potential energy diagrams obtained at the CCSD(T)//BHandHLYP/6-311++G(d,p) level are also given below. The moments of inertia and vibrational frequencies of the reactants, reactant complexes, transition states, and product complexes used in the rate constant calculations are presented in Table S1 of the Supporting Information. Relative energies of all the species in the three different reaction systems are shown in Tables S2, S3, and S4 in the Supporting Information. As for **RC−Zc**, which is a reactant complex in the reaction of (*Z*)-1-propenol with OH, we used the PMP2/aug-cc-pVTZ//BHandHLYP/6-311++G(d,p) method to obtain the relative energy, because single-point coupled cluster calculations failed to give a reasonable energy for this complex, due in part to high spin contamination of the wave function. The T1 diagnostic value in CCSD(T) calculations of **RC−Zc** significantly exceeded 0.02 (close to 0.08) signaling unreliability of the CCSD(T) result. This is not unusual, as Alvarez-Idaboy[11] and Sekušak et al.[38] made similar observations for the OH + alkenes reactions and OH + aldehydes reactions, respectively. Thus, just for this entrance complex, the PMP2 results removing spin contamination are expected to be more reliable.

(E)-1-Propenol + OH System. The optimized geometries of the species for the reaction of OH + (*E*)-1-propenol are shown in Figure 1, and the potential energy diagrams obtained at the CCSD(T)//BHandHLYP/6-311++G(d,p) level are given in Figure 2. Two reactant complexes (**RC−Ea** and **RC−Eb** in Figure 1) are identified in this reaction process. The formation of **RC−Ea**, 6.3 kcal/mol lower than the reactants, is caused by the interaction between the H atom of OH radical and the O atom of (*E*)-1-propenol, at a distance of 1.893 Å, which represents a hydrogen bond and is responsible for the stabilization. The formation of **RC−Eb**, 8.2 kcal/mol lower than the reactants, is caused by a hydrogen bond between the O atom of OH radical and the H atom of the OH group in (*E*)-1-propenol at 2.013 Å. Meanwhile, we also studied the isomerization process from (*E*)-1-propenol to (*Z*)-1-propenol. The transition state for this process (TS-EZ) lying 67.44 kcal/mol above (*E*)-1-propenol is shown in Figure 1. One can see that the barrier for this process is high enough to distinguish the two isomers even at high temperatures because the isomerization occurs by rotation around a double C=C bond.

Two transition states were found from the initial reactant complex of **RC-Ea**: $HOCHCHCH_2(H\cdots OH)$ (**TS-E1**) and $CH_3CHC(H\cdots OH)OH$ (**TS-E3**), in which different H atoms are abstracted from (*E*)-1-propenol (Figure 1). In **TS-E1**, the OH radical directly abstracts an H atom from the CH_3 group. The breaking C−H bond in the transition state is 0.094 Å longer than that in the reactant. **TS-E1** has one imaginary frequency of 934*i* cm^{-1}, lies 6.2 kcal/mol above **RC-Ea**, and leads to the formation of the product complex **PC-E1**, 31.2 kcal/mol below the reactants in the exit channel. The product complex **PC-E1** is stabilized due to the attractive interaction between the O atom in the water molecule and an H atom in the CH_2 group at a distance of 2.416 Å. In **TS-E3**, the OH radical abstracts the H atom from the CH group. The breaking C−H bond in **TS-E3** is 0.184 Å longer than that in the reactant. **TS-E3** with an imaginary frequency of 2005*i* cm^{-1} represents a distinct transition state lying 10.6 kcal/mol above **RC-Ea** and leading to the formation of the product complex **PC-E3**, which resides 16.4 kcal/mol below the reactants. The stabilization of **PC-E3** can be attributed to the attractive interaction between the O atom in H_2O and the H atom in the OH group at a distance of 1.800 Å.

Similarly, two transition states were found from the initial reactant complex of **RC-Eb**: $CH_3C(H\cdots OH)CHOH$ (**TS-E2**) and $CH_3CHCHO(H\cdots OH)$ (**TS-E4**), both for abstraction of different H atoms from (*E*)-1-propenol (Figure 1). In **TS-E2**, the OH radical abstracts the H atom from the CH group and the breaking C−H bond is 0.374 Å longer than that in the reactant. The calculated barrier at **TS-E2** is 12.2 kcal/mol relative to **RC-Eb**, with an imaginary frequency of 1480*i* cm^{-1}, and the H abstraction process results in the formation of the product complex **PC-E2**, 13.7 kcal/mol below the reactants. The complex is stabilized by hydrogen bonding between the O atom of water the H atom in the OH group at 1.866 Å. In **TS-E4**, the OH radical abstracts the H atom from OH. The cleaving O−H bond is 0.072 Å longer than that in the reactant. **TS-E4** exhibits one imaginary frequency of 2592*i* cm^{-1}, lies 8.3 kcal/mol above **RC-Eb**, and leads to the formation of the product complex **PC-E4**, 42.2 kcal/mol lower in energy than the reactants. **PC-E4** possesses a ringlike structure (Figure 1) and is stabilized by two hydrogen bonds, the strongest of which occurs between an H atom H_2O and the O atom in the CHO group at a distance of 1.929 Å.

The radical products corresponding to all the abstraction pathways are also shown in Figure 1. One can see that their geometries remain nearly unchanged as compared to the corresponding product complexes.

(Z)-1-Propenol + OH System. The optimized geometries of the species for this reaction are given Figure 3. Three reactant complexes, **RC-Za**, **RC-Zb**, and **RC-Zc**, are found in the reaction entrance channel. Their relative energies with respect to the reactants are illustrated in Figure 4. **RC-Za** is formed by a typical hydrogen bond interaction between the H atom of the OH radical and the O atom in (*Z*)-1-propenol at the distance of 1.893 Å. **RC-Zb** is stabilized by the interaction between OH and the CC double bond in (*Z*)-1-propenol, with the distance between the O atom and the central C atom being 2.418 Å (Figure 3). The formation of **RC-Zc** is attributed to the interaction between the O atom in the OH radical and the H atom in the OH group of (*Z*)-1-propenol. The distance between the two atoms is 2.056 Å, which is also typical for a hydrogen bond interaction.

Four transition states are identified in this case, $CH_2(H\cdots OH)CHCHOH$ (**TS-Z1**), $CH_3C(H\cdots OH)CHOH$ (**TS-Z2**), $CH_3CHC(H\cdots OH)OH$ (**TS-Z3**), and $CH_3CHCHO(H\cdots OH)$ (**TS-Z4**), corresponding to different H atom abstraction pathways from (*Z*)-1-propenol. The transition state **TS-Z1** has a ringlike structure and is connected to the reactant complex **RC-Zc**. **TS-Z1** lies only 0.8 kcal/mol above **RC-Zc** and has an imaginary frequency of 952*i* cm^{-1}. It corresponds to the direct H atom abstraction by OH from the CH_3 group. This leads to the formation of **PC-Z1**, which lies 37.0 kcal/mol below the initial reactants. On the other hand, the transition state **TS-Z4** can also be formed from the reactant complex **RC-Zc** by moving

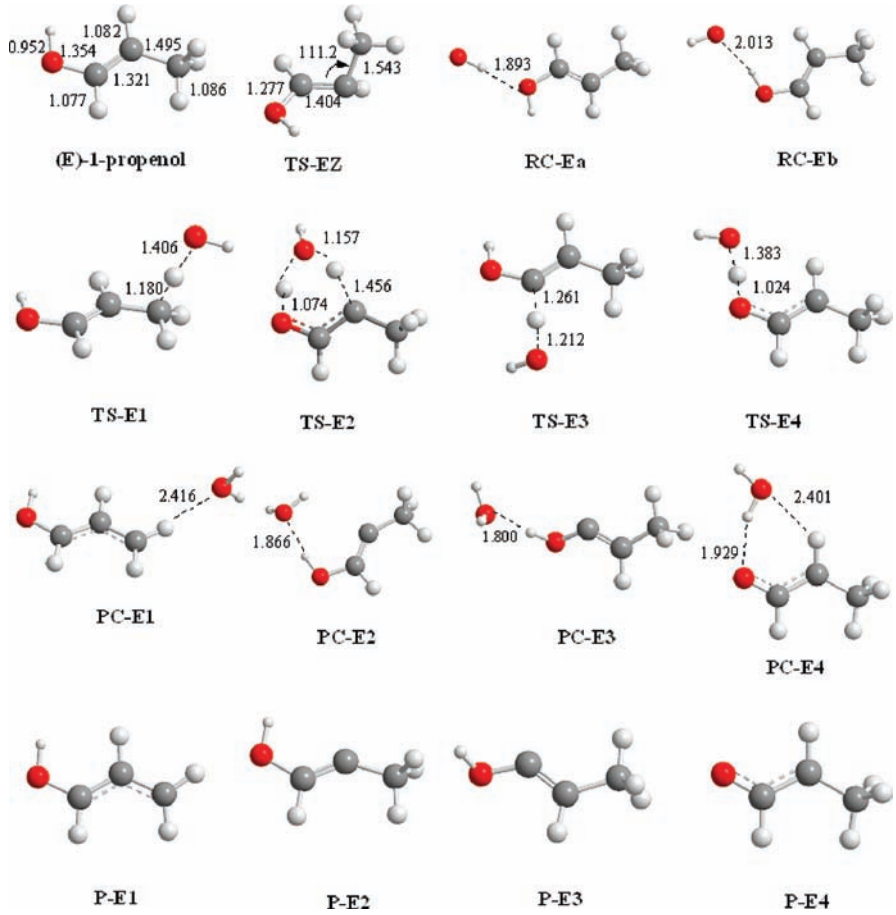

Figure 1. Geometries of the reactant, reactant complexes, transition states, product complexes, and products involved in the OH + (*E*)-1-propenol reaction optimized at the BHandHLYP/6-311++G(d,p) level.

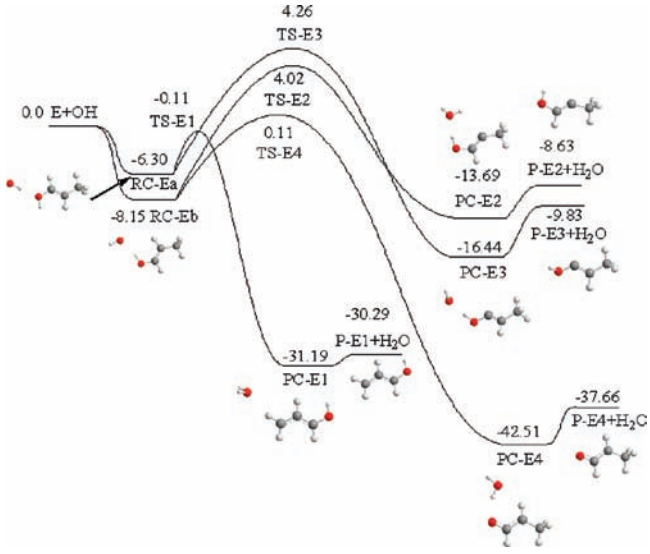

Figure 2. Potential energy diagram for the OH + (*E*)-1-propenol reaction calculated at the CCSD(T)//BHandHLYP/6-311++G(d,p) level.

the OH radical toward the OH group in (*Z*)-1-propenol. The breaking O−H bond in this transition state is 0.074 Å longer than that in the reactant. **TS-Z4** has one imaginary frequency of 2487*i* cm^{-1}, lies 2.9 kcal/mol above **RC-Zc**, and is connected to the product complex **PC-Z4**, 38.2 kcal/mol below the reactants. **TS-Z2** and **TS-Z3**, which are formed from the reactant complexes **RC-Zb** and **RC-Za**, correspond to H abstractions from two distinct CH groups in (*Z*)-1-propenol with barriers of

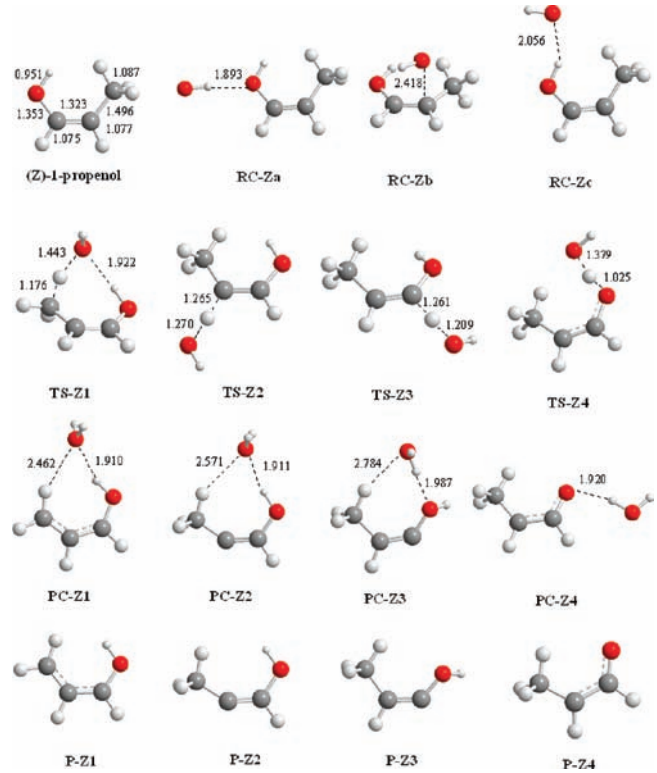

Figure 3. Geometries of the reactant, reactant complexes, transition states, product complexes, and products involved in the OH + (*Z*)-1-propenol reaction optimized at the BHandHLYP/6-311++G(d,p) level.

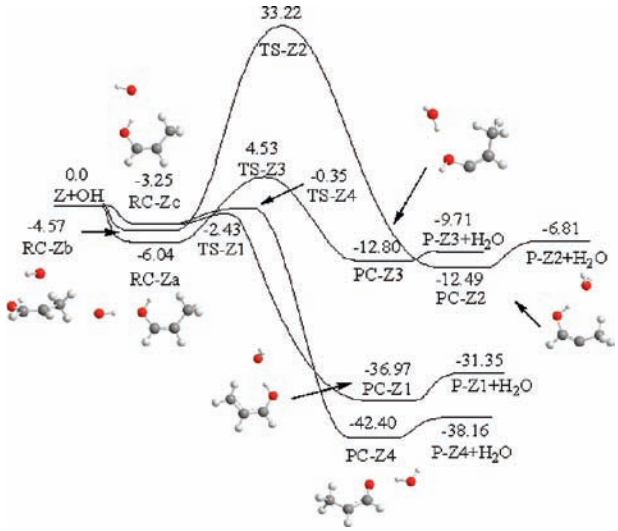

Figure 4. Potential energy diagram for the reaction of OH + (*Z*)-1-propenol calculated at the CCSD(T)//BHandHLYP/6-311++G(d,p) level.

37.8 and 9.1 kcal/mol, respectively. These processes lead to the product complexes **PC-Z2** and **PC-Z3**, with relative energies of 6.8 and 9.7 kcal/mol below the reactants, respectively.

The formation and stabilization of **PC**s can be attributed to the attractive interaction between O and H atoms forming a variety of hydrogen bonds. For instance, in **PC-Z1** and **PC-Z2** the hydrogen bonds are created between the O atom of the water molecule and the H atom in the OH group, whereas in **PC-Z3** and **PC-Z4** the bonds are formed between an H atom in H_2O and the O atom of the products. For the **PC-Z1**, **PC-Z2**, and **PC-Z3** complexes, we can also see in Figure 3 other bonding interactions between O in H_2O and one of the H atoms in the products. The O···H distances in this case are in the range of 2.5−2.8 Å, which is rather long for a hydrogen bond contact. Apparently, these bonds are weak because hydrogen atoms linked to carbons do not bear sufficient positive charge to strongly interact with an O atom.

The radical products corresponding to all abstraction pathways are also shown in Figure 3 with their geometries remaining nearly unchanged as compared to the corresponding product complexes. From Figure 4, we can see that the radical products have higher energies than the corresponding product complexes, and the channel leading to **P-Z2** + H_2O is not expected to be kinetically important in a lower temperature range because of its much higher barrier compared to the other three channels.

***syn*-Propen-2-ol + OH System.** As shown in Figure 5, three reactant complexes (**RC-Sa**, **RC-Sb**, and **RC-Sc**) are identified in the entrance channel of this reaction. Among them, **RC-Sa** and **RC-Sb** are stabilized by typical hydrogen bonds with lengths of 1.901 and 2.010 Å, respectively. The **RC-Sc** reactant complex, where the OH radical is almost perpendicular to the CC double bond with the positively charged H atom pointing toward the double bond, is formed through the interaction between the OH hydrogen atom and the π-electron density of the double bond in *syn*-propen-2-ol. The relative energies of the complexes with respect to the reactants are depicted in Figure 6.

Three transition states CH_2(H···OH)$COHCH_2$ (**TS-S1**), CH_3COHCH(H···OH) (**TS-S2**), and CH_3CO(H···OH)CH_2 (**TS-S3**) are shown in Figure 5, corresponding to different H atom abstraction channels from *syn*-propen-2-ol. OH radical abstracts an H atom of the CH_3 group through the transition state **TS-S1**

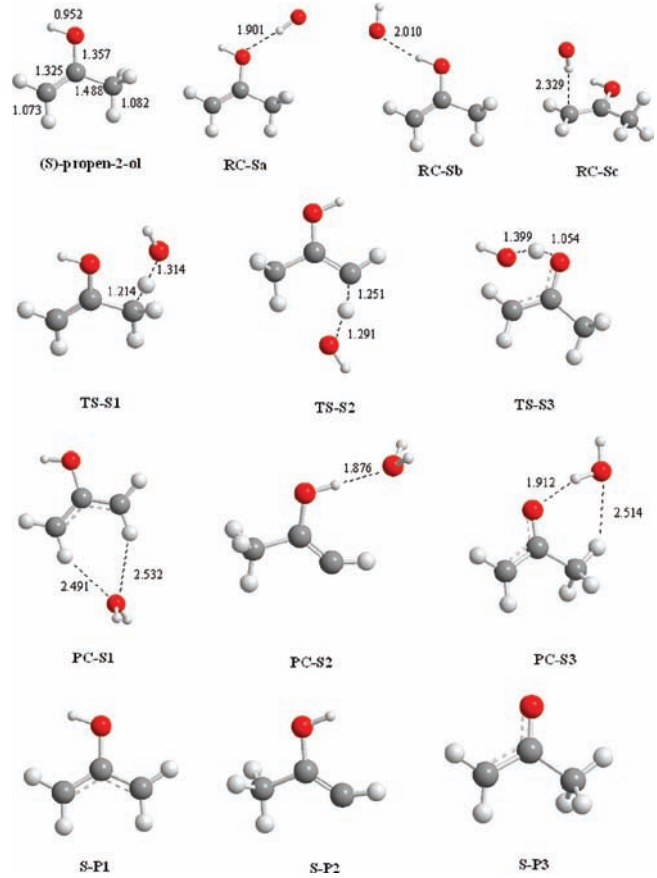

Figure 5. Geometries of the reactant, reactant complexes, transition states, product complexes, and products involved in the OH + *syn*-propen-2-ol reaction optimized at the BHandHLYP/6-311++G(d,p) level.

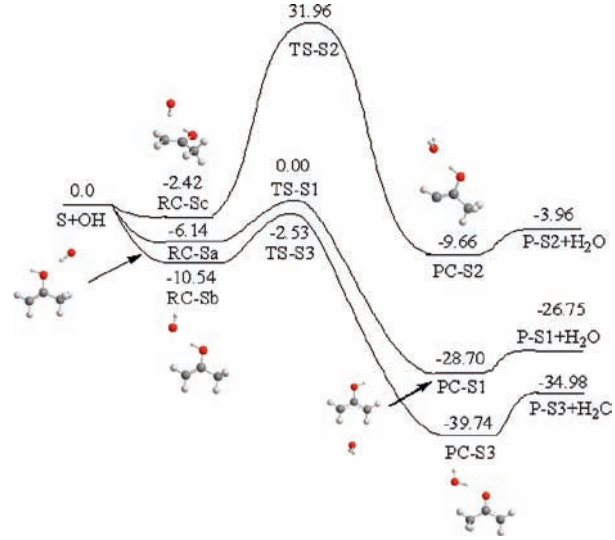

Figure 6. Potential energy diagram for the reaction of OH + *syn*-propen-2-ol calculated at the CCSD(T)//BHandHLYP/6-311++G(d,p) level.

lying 6.1 kcal/mol above **RC-Sa**, which leads to the formation of **PC-S1**, 28.7 kcal/mol below the OH + *syn*-propen-2-ol reactants. Abstraction of a hydrogen atom in the CH_2 group by OH occurs via **TS-S2**. The breaking C−H bond in this transition state is 0.178 Å longer than that in the reactant. **TS-S2** possesses an imaginary frequency of 3624*i* cm^{-1}, lies 34.38 kcal/mol above **RC-Sc**, and leads to the creation of the product complex **PC-S2**, 9.7 kcal/mol below the reactants. Similarly, H atom

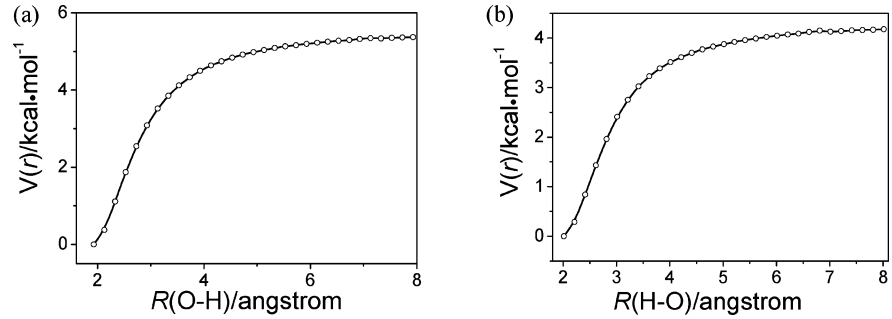

Figure 7. Morse curves for two different entrance channels in the (*E*)-1-propenol + OH reaction system: (a) (*E*)-1-propenol + OH → RC-Ea; (b) (E)-1-propenol + OH → RC-Eb. Open circles are computed at the BHandHLYP/6-311++G(d,p) level, and solid curves are the fitted Morse function.

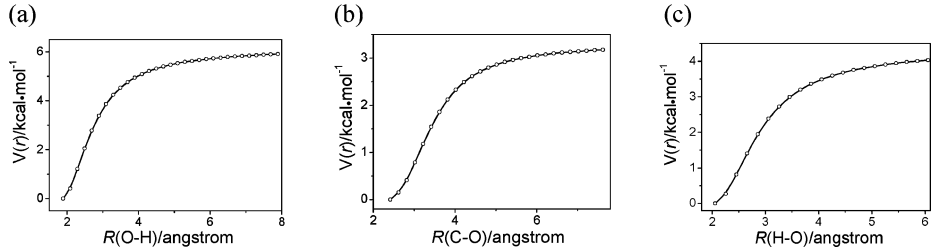

Figure 8. Morse curves for three different entrance channels in the (*Z*)-1-propenol + OH reaction system: (a) (*Z*)-1-propenol + OH → RC-Za; (b) (*Z*)-1-propenol + OH → RC-Zb; (c) (*Z*)-1-propenol + OH → RC-Zc. Open circles are computed at the BHandHLYP/6-311++G(d,p) level, and solid curves are the fitted Morse functions.

abstraction from the OH group proceeds through the transition state **TS-S3** with an imaginary frequency of 1217*i* cm^{-1}, lying 8.0 kcal/mol above **RC-Sb**. This results in the formation of **PC-S3**, which resides 39.7 kcal/mol lower in energy than OH + *syn*-propen-2-ol. The O···H distance in **PC-S1** is about 2.5 Å, indicating a weak hydrogen bond interaction.

We can see again (Figure 6) that the energies of the radical products are higher than those for the corresponding product complexes. A comparison of the three different channels shows that the two channels leading to the **PC-S1** + H_2O and **PC-S3** + H_2O products are more competitive because of their lower activation barriers.

B. Rate Constants and Product Branching Ratios. In this section, we compute rate constants for all channels in different reaction systems discussed above. We carry out the variational TST and RRKM calculations based on the PES and mechanisms presented in the preceding sections. The Variflex code by Klippenstein et al.[32] is employed for this purpose, in the temperature range 200−3000 K at pressures of 1 and 100 atm of the N_2 bath gas. The energy transfer behavior is assumed to be governed by weak molecular collisions, and the collision frequency is derived from the Lennard-Jones (L-J) pairwise potential with parameters of N_2 [$\sigma(N_2) = 3.738$ Å, $\varepsilon/k_B(N_2) = 82.0$ K] and $CH_3CO_2CH_3$ [$\sigma(CH_3CO_2CH_3) = 5.141$ Å, $\varepsilon/k_B(CH_3CO_2CH_3) = 389.4$ K].[39] These values are employed for evaluation of the L-J parameters for each collision pair using the approximations $\sigma_{12} = (\sigma_1 + \sigma_2)/2$ and $\varepsilon_{12} = (\varepsilon_1\varepsilon_2)^{1/2}$. The energy transfer per downward collision, $\langle\Delta E_{down}\rangle$, is assumed to be 200 cm^{-1} in N_2 following the work by Zhu et al.[40] The energies given in Figures 2, 4, and 6, along with rotational constants and the vibrational frequencies presented in Table S1 in the Supporting Information are used here to calculate the rate constants for the corresponding reaction systems. For the reaction without a well-defined transition states, the Morse potential $E(R) = D_e[1 - \exp\{-\beta(R - R_e)\}]^2$ was used to represent the potential energy along the individual reaction coordinate. In the above equation, D_e is the bond energy excluding zero-point energy, R is the reaction coordinate (i.e., the distance between the two bonding atoms), and R_e is the equilibrium value of R. The Lennard-Jones pairwise potential and the anisotropic potential (a potential anisotropy form assuming a bending potential which is cylindrically symmetric with respect to each fragment) are added together to form the final potential for the variational rate constant calculations by the Variflex code. The number of states for tight transition states is evaluated according to the rigid-rotor harmonic-oscillator assumption employed in the Variflex code.[41] Meanwhile, the anharmonic effect of low-frequency vibrational modes has been treated by the hindered rotor approximation in the whole temperature range. According to Sansón et al.,[42] if soft low-frequency modes behaving like hindered rotors are treated anharmonically but higher frequency modes are treated within the harmonic approximation, the deviations of the calculated rate constants from those obtained using the fully anharmonic treatment do not exceed 30%, and thus the anharmonicity has a relatively small effect on the rate constants. The quantum tunneling effects are included when necessary using the Eckart tunneling model.[43]

We take the **RC**s in all reaction systems as reacting complexes in the rate constant calculations with Variflex. The Morse potentials mentioned above are used to represent the barrierless processes from the reactants to the corresponding reactant complexes. In the reaction of OH with (*E*)-1-propenol, two barrierless processes forming the complexes of RC-Ea, and RC-Eb are taken into consideration, the Morse curves for these processes are shown in Figure 7. In the reaction of OH with (*Z*)-1-propenol, three barrierless entrance processes forming the complexes of RC-Za, RC-Zb, and RC-Zc are investigated, and the Morse curves for these process are shown in Figure 8. In the reaction of OH with *syn*-propen-2-ol, three barrierless entrance processes to form the complexes of RC-Sa, RC-Sb, and RC-Sc are studied, and the Morse curves are shown in Figure 9. The fitted parameters for all the processes mentioned above are listed in Table 1. The pathways for the three different reaction systems are illustrated in Schemes 1, 2, and 3, respectively, where E, Z, and S represent (*E*)-1-propenol, (*Z*)-

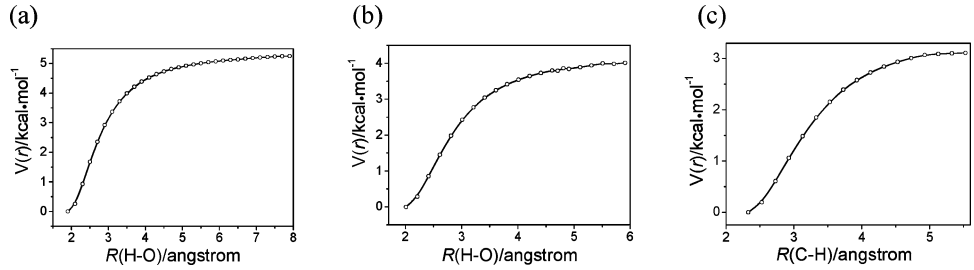

Figure 9. Morse curves for three different entrance channels in the OH + *syn*-propen-2-ol reaction system: (a) *syn*-propen-2-ol + OH → RC-Sa; (b) *syn*-propen-2-ol + OH → RC-Sb; (c) *syn*-propen-2-ol + OH → RC-Sc. Open circles are computed at the BHandHLYP/6-311++G(d,p) level, and solid curves are the fitted Morse functions.

TABLE 1: Fitted Morse Potential Parameters for Different Processes

barrierless processes	D_e (kcal/mol)	β (Å^{-1})
(*E*)-1-propenol + OH → RC-Ea	5.24	1.407
(*E*)-1-propenol + OH → RC-Eb	4.08	1.411
(*Z*)-1-propenol + OH → RC-Za	5.75	1.409
(*Z*)-1-Propenol + OH → RC-Zb	3.16	1.199
(*Z*)-1-Propenol + OH → RC-Zc	3.97	1.465
syn-propen-2-ol + OH → RC-Sa	5.13	1.353
syn-propen-2-ol + OH → RC-Sb	3.97	1.507
syn-propen-2-ol + OH → RC-Sc	3.20	1.428

SCHEME 1

k_1: E + OH ⇌ RC-Ea

k_2: E + OH ⇌ RC-Ea ⇌ PC-E1 → E-P1 + H_2O

k_3: E + OH ⇌ RC-Ea ⇌ PC-E3 → E-P3 + H_2O

k_4: E + OH ⇌ RC-Eb

k_5: E + OH ⇌ RC-Eb ⇌ PC-E2 → E-P2 + H_2O

k_6: E + OH ⇌ RC-Eb ⇌ PC-E4 → E-P4 + H_2O

SCHEME 2

k_1': Z + OH ⇌ RC-Za

k_2': Z + OH ⇌ RC-Za ⇌ PC-Z3 → Z-P3 + H_2O

k_3': Z + OH ⇌ RC-Zb

k_4': Z + OH ⇌ RC-Zb ⇌ PC-Z2 → Z-P2 + H_2O

k_5': Z + OH ⇌ RC-Zc

k_6': Z + OH ⇌ RC-Zc ⇌ PC-Z1 → Z-P1 + H_2O

k_7': Z + OH ⇌ RC-Zc ⇌ PC-Z4 → Z-P4 + H_2O

SCHEME 3

k_1'': S + OH ⇌ RC-Sa

k_2'': S + OH ⇌ RC-Sa ⇌ PC-S1 → S-P1 + H_2O

k_3'': S + OH ⇌ RC-Sb

k_4'': S + OH ⇌ RC-Sb ⇌ PC-S3 → S-P3 + H_2O

k_5'': S + OH ⇌ RC-Sc

k_6'': S + OH ⇌ RC-Sc ⇌ PC-S2 → S-P2 + H_2O

1-propenol, and *syn*-propen-2-ol, respectively. We also assume that once the product complexes are formed, they can easily dissociate to the products; the assumption is justified by the fact that the binding energies of these complexes are much lower than the reverse H abstraction barriers.

(E)-1-Propenol + OH System. The Arrhenius plots showing temperature dependence of the predicted total and individual rate constants for (*E*)-1-propenol + OH are presented in Figure 10a at 1 atm and Figure 10b at 100 atm pressures. The predicted total rate constant represents the sum of the rate constants for the six channels shown in Scheme 1. Experimental values for these channels are not available. As shown in Figure 10, the predicted total rate constants decrease with the increasing temperature in the low temperature range (200 K < T < 700 K) and increase with the temperature increase in the high temperature range (700 K < T < 3000 K). The marked change in the apparent activation energy reflects a change of the rate-determining reaction step, from the reactant complex formation channel below 700 K to the hydrogen abstraction channels above 700 K. As expected of barrierless complex formation processes, both k_1 and k_4 show negative temperature dependence. Especially when the temperature is higher than 500 K, these rate constants greatly decrease because the reactant complex stabilization channels become unimportant due to the extremely rapid decomposition rate of RC-Ea and RC-Eb back to the reactants. This tendency is consistent with the results for analogous processes in the reaction of OH with ethene calculated by Senosiain et al.[44] and in the reaction of OH with propene calculated by us.[8] The lower energy of RC-Eb makes rate constants for its formation higher as compared to those for RC-Ea. As shown in Figure 8a, for the other four channels, the inequality $k_2 \approx k_6 > k_3 > k_5$ holds across the temperature range of 200−3000 K, which can also be predicted from the barriers for these channels. According to the potential energy diagram (Figure 2), the barrier at TS-E2 for the channel 2 is lower than that at TS-E4 for the reaction 6 by 2.0 kcal/mol. However, the inequality $k_2 < k_6$ holds in the temperature range of 200 K < T < 2000 K, whereas $k_2 > k_6$ holds in the higher temperature range of 2000 K < T < 3000 K; this may result from faster formation of RC-Eb compared to RC-Ea. At 100 atm (see Figure 10b), the values of k_1 and k_4 are almost the same as those calculated for 1 atm. Obviously, the inequality $k_2 > k_6 > k_3 > k_5$ holds across the temperature range of 200−3000 K, except for the fact that k_2 is very close to k_6 in the temperature range 400 K < T < 3000 K.

Channel switching is the cause of the curvature in the plot of the total rate constant. The product branching ratios based on the theoretical rate constants computed at 1 atm of N_2 are presented in Figure 11 as functions of temperature. It is apparent that the complexes RC-Ea and RC-Eb are the dominant products under ~350 K. The contribution of the two channels is almost 99% at 200 K and 80% at 350 K. Then, the two branching ratios decrease rapidly from 350 to 600 K. The branching ratio

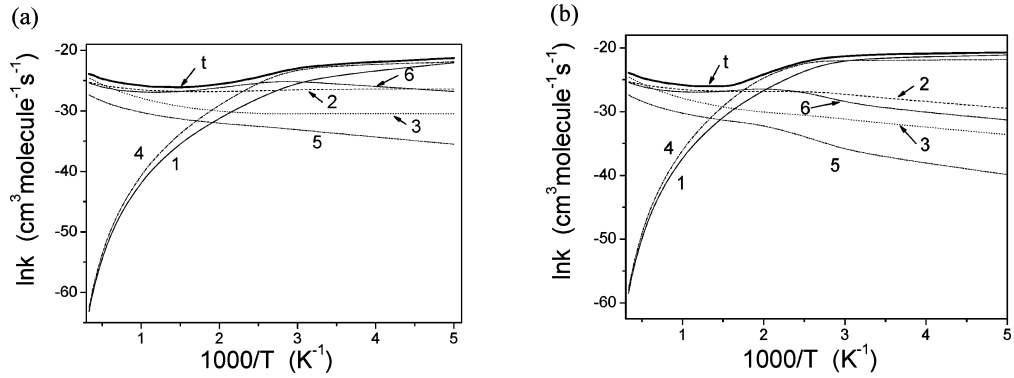

Figure 10. Temperature dependence of rate constants at (a) 1 atm and (b) 100 atm for the channels 1−6 in the reaction of OH + (*E*)-1-propenol. The numbers refer to individual reaction channels and "t" denotes the total rate constant.

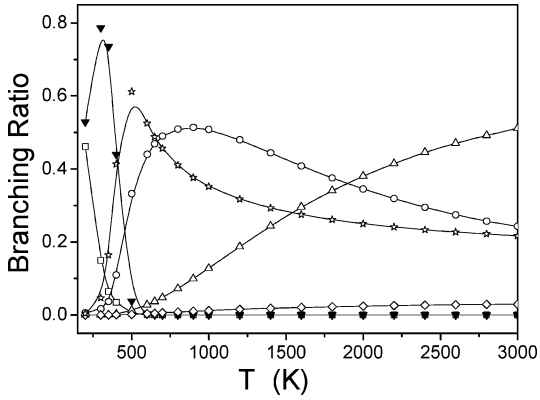

Figure 11. Product branching ratios in the OH + (E)-1-Propenol reaction at 1 atm of N_2 diluent. The lines with symbols represent the following: □, RC-Ea; ○, PC-E1; △, PC-E3; ▼, RC-Eb; ◇, PC-E2; ☆, PC-E4.

of PC-E4 increases steeply from 200 to 500 K and decreases slowly from 500 to 3000 K becoming 22% at 3000 K. The branching ratio of PC-E1 increases rapidly from 500 to 900 K and then decreases slowly from 900 to 3000 K reaching 24% at 3000 K. The branching ratio of PC-E3 increases in the whole temperature range, and this product becomes most favorable above 2000 K, with 51% at 3000 K. The branching ratio of PC-E2 is too small to compete throughout the entire temperature range investigated.

(Z)-1-Propenol + OH System. Panels a and b of Figure 12 show the total and individual rate constants predicted at 1 and 100 atm, respectively, for (*Z*)-1-propenol + OH. Here, the total rate constant is the sum of the seven channel rate constants shown in Scheme 2. We can see that the computed total rate constant decreases with temperature at 200 K < T < 700 K and then increases at 700 K < T < 3000 K. Dominant channel switching is again the cause of the observed curvature in the total rate constant, similar to the OH + (*E*)-1-propenol reaction system. At 1 atm, the three entrance barrierless channels k_1', k_3', and k_5' show negative temperature dependence. They are fastest below 500 K, but when the temperature is higher than 500 K, the three rate constants decrease steeply. At 1 atm, we observe $k_6' \approx k_7' > k_2' > k_4'$ in the temperature range 200 K < T < 900 K. Looking at the energy diagram in Figure 4, one can see that even though the energy barrier for the channel 7′ is higher than that for the channel 6′ by about 2.0 kcal/mol, both rate constants are very close in the whole temperature range. The inequality mentioned above does not hold when the temperature is higher than 900 K. The rate constant of channel 2′, k_2', becomes larger than both k_6' and k_7' when T is higher than 900 K and k_4' overtakes k_2' above 2000 K.

The temperature dependence of calculated branching ratios is illustrated in Figure 13. It is evident that the entrance channel producing RC-Za is predominant in the lower temperature range from 200 to 400 K, but its significance decreases rapidly above 400 K. The branching ratio of this channel reaches its maximum of 91% at 350 K and falls to 2% at 500 K. The other two entrance channels producing RC-Zb and RC-Zc are minor as their branching ratios do not exceed 2% at 500 K. The branching ratio of PC-Z1 greatly increases from 300 to 650 K and reaches 70% at 650 K. Then it rapidly decreases, becoming nearly zero at 3000 K. The branching ratio of PC-Z3 gradually increases with temperature, from 2% at 500 K to 45.1% at 1400 K, and then slowly decreases when the temperature is higher than 1400 K, falling to 7.2% at 3000 K. The branching ratio of PC-Z2 increases within the whole temperature range investigated, with

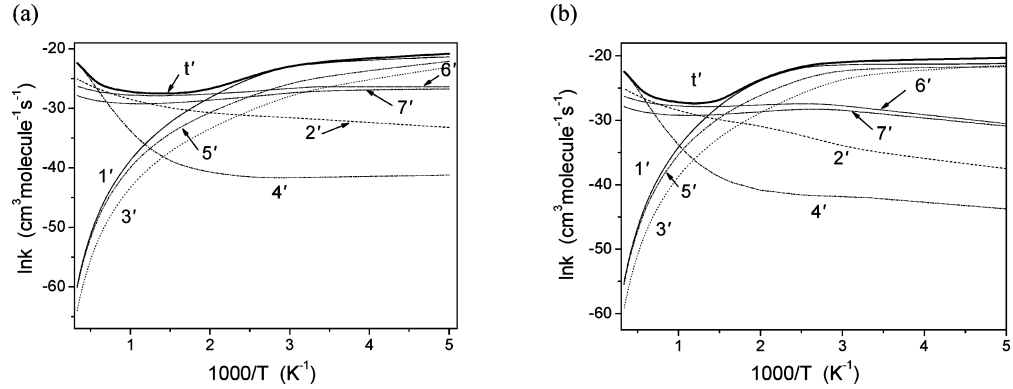

Figure 12. Temperature dependence of rate constants at (a) 1 atm and (b) 100 atm for channels 1′−7′ in the reaction of OH + (*Z*)-1-propenol. The numbers refer to individual channels and t′ denotes the total rate constant.

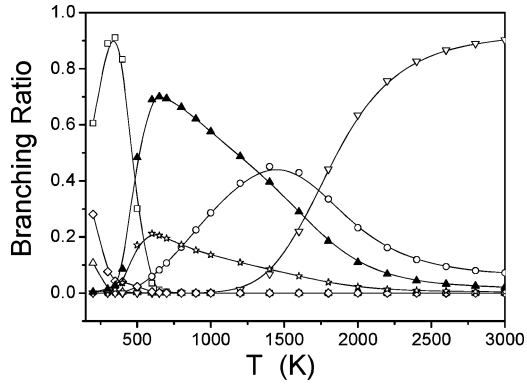

Figure 13. Product branching ratios in the OH + (*Z*)-1-propenol reaction at 1 atm of N_2 diluent. The lines with symbols represent the following: □, RC-Za; ○, PC-Z3; △, RC-Zb; ▽, PC-Z2; ◇, RC-Zc; ▼, PC-Z1; ☆, PC-Z4.

this channel becoming dominant above 1800 K and rising to 90.3% at 3000 K.

syn-Propen-2-ol + OH System. Temperature dependence of the predicted total and individual rate constants for OH + *syn*-propen-2-ol are shown in Figure 14a at 1 atm and Figure 14b at 100 atm. The total rate constant is the sum of the six channel rate constants shown in Scheme 3. Obviously, the total rate constant exhibits curvature similar to those observed for OH + (*E*)-1-propenol and OH + (*Z*)-1-propenol and caused by the same reason. Rate constants k_1'', k_3'', and k_5'' for the three barrierless entrance channels producing RC-Sa, RC-Sb, and RC-Sc show negative temperature dependence. The rate constant k_6'' for the step producing PC-S2 is not competitive within the whole temperature range and can be ignored. Below 500 K, channel 2″ should be more favorable than channel 4″, but they become competitive as the temperature increases and have similar rates in the whole higher temperature range (500 K < T < 3000 K).

On the basis of the individual product channel rate constants discussed above, branching ratios have been evaluated and graphically presented in Figure 15. The channels leading to RC-Sc and PC-S2 are too slow to be competitive throughout the entire investigated temperature range, so their relative yields are not included in Figure 15. It is evident that the channels producing RC-Sa and RC-Sb are predominant up to 500 K, and then their branching ratios rapidly decrease. From 500 to 900 K, branching ratios of the other two channels forming PC-S1 and PC-S3 increase steeply and become very significant. Above 900 K, the PC-S1 product becomes dominant with its relative yield reaching 51.7% at 900 K and 70.5% at 3000 K, whereas the ratio of PC-S3 is 48% and 29.5% at 900 and 3000 K, respectively.

To provide the reaction rate constants for the use in chemical kinetics modeling, we fitted the total rate constants of the three reaction systems to modified three-parameter Arrhenius expressions. As the plots of the three total rate constants in Figures 10, 12, and 14 are curved, we fitted their values at the pressure of 1 atm in two different temperature ranges. The results in units of $cm^3molecule^{-1}s^{-1}$ are as the following:

OH + (*E*)-1-propenol:

$$k_{200-700} = (2.23 \pm 0.38)T^{(-4.18\pm0.25)} \exp((49 \pm 10)/T)$$

$$k_{700-3000} = (1.22 \pm 0.92) \times 10^{-21}T^{(2.73\pm0.12)} \exp((1558 \pm 59.5)/T)$$

OH + (*Z*)-1-propenol:

$$k_{200-700} = (1.18 \pm 0.85) \times 10^{8}T^{-7.33} \exp((-448 \pm 8.96)/T)$$

$$k_{700-3000} = (2.33 \pm 0.12) \times 10^{-43}T^{9.17\pm0.37} \exp((7446 \pm 99.7)/T)$$

OH + *syn*-propen-2-ol:

$$k_{200-800} = (1.72 \times 10^{29})T^{-12.79\pm0.19} \exp((-3099 \pm 29.3)/T)$$

$$k_{800-3000} = (2.21 \pm 1.6) \times 10^{-21}T^{2.73\pm0.11} \exp((2042 \pm 58.8)/T)$$

C. OH Addition Channels. Since the propenol isomers have a double C═C bond, other possible reaction channels not considered so far may involve OH addition to this double bond. In this section we briefly study one such OH addition channel for (*E*)-1-propenol in order to evaluate its relative importance as compared to H abstractions. The calculated potential energy diagram is illustrated in Figure 16. One can see that the reactant complex (RC-E-add) bound by 6.0 kcal/mol can be formed from the reactants through a barrierless process. Then, the addition intermediate IM-E-add lying 32.0 kcal/mol below the initial OH + (*E*)-1-propenol reactants can be produced through the transition state TS-E-add. The calculated barrier for this process is 0.7 kcal/mol, which is significantly lower as compared to the barriers for the H-abstraction channels in the OH + (*E*)-1-propenol reaction. According to our rate constants calculations for the OH + propene reaction system, which showed similar energetic parameters for the OH addition and H abstraction pathways, the addition channels are dominant at lower temperatures, whereas the H abstraction channels take over in the higher temperature range above 1000 K.[8] An analogous behavior can be also expected for the OH reactions with propenol isomers. Therefore, the OH addition channels need to be carefully investigated to obtain reliable predictions of the reaction rate constants at low temperatures for atmospheric chemistry applications. As our main interest in the present work is to evaluate high-temperature rate constants relevant to combustion, a detailed account of the addition channels will be given in a future publication.

4. Conclusions

The reaction mechanism and kinetics of the OH abstraction reactions from propenols have been investigated within a stepwise mechanism involving the formation of a reactant complex in the entrance channel and a product complex in the exit channel. Three stable conformers of propenols, (*E*)-1-propenol, (*Z*)-1-propenol, and *syn*-propen-2-ol, have been taken into consideration and, for each of them, H abstractions from all different sites have been studied. The rate constants are calculated in the temperature range of 200−3000 K using the

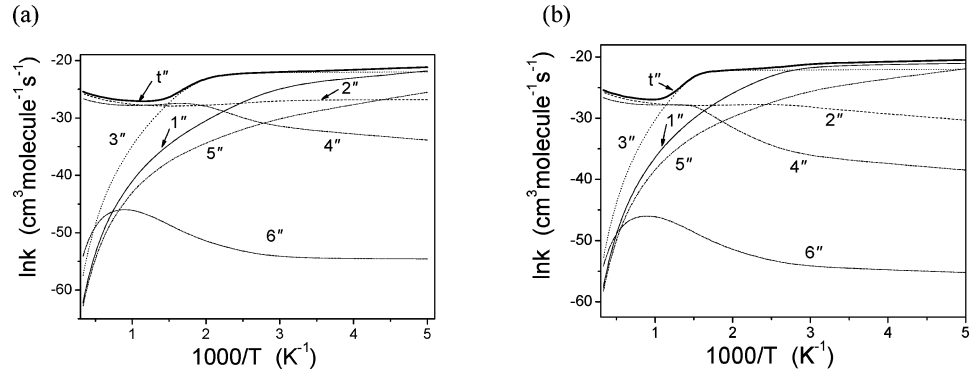

Figure 14. Temperature dependence of rate constants at (a) 1 atm and (b) 100 atm for channels 1′−6″ in the reaction of OH + *syn*-propen-2-ol. The numbers refer to individual channels and t″ denotes the total rate constants.

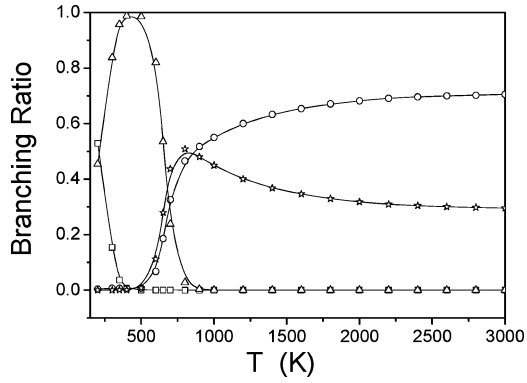

Figure 15. Product branching ratios in the OH + *syn*-propen-2-ol reaction at 1 atm of N_2 diluent. The lines with symbols represent the following: □, RC-Sa; ○, PC-S1; △, RC-Sb; ☆, PC-S3.

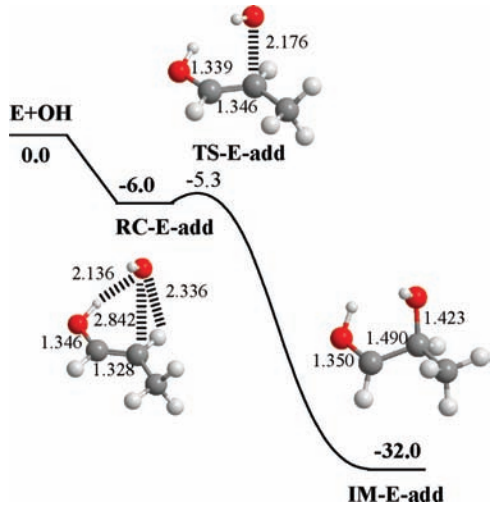

Figure 16. Potential energy diagram for the central addition channel in the OH + (*E*)-1-propenol reaction calculated at the CCSD(T)//BHandHLYP/6-311++G(d,p) level.

Variflex code, based on the weak collision master equation/microcanonical variational RRKM theory including tunneling corrections.

The results show that in the reaction of OH with (*E*)-1-propenol, the abstractions from the $-CH_3$ and $-OH$ sites are dominant and competitive with each other in the temperature range from 500 to 2000 K. Above 2000 K, the abstraction from the $-CH$ group linked to the O atom becomes more important with the yield reaching 51.1% at 3000 K. The abstraction from the $-CH$ site bonded to the CH_3 group is a minor channel through the whole temperature range investigated and can be ignored. In the reaction of OH with (*Z*)-1-propenol, the abstractions from the $-CH_3$ site, the $-CH$ site bonded to the O atom, and the $-OH$ site are preferable in the temperature range from 500 to 1800 K, and the first two channels are competitive with each other. When the temperature exceeds 1800 K, the hydrogen abstraction reaction from the CH group bonded to CH_3 becomes dominant with 90.3% at 3000 K. In the reaction of OH with *syn*-propen-2-ol, the abstractions from the $-CH_3$ and OH sites are competitive with each other when temperature is higher than 500 K, and they become favorable reaction channels above 800 K with branching ratios reaching 70.5% and 29.5% at 3000 K, respectively. The hydrogen abstraction reaction from the $-CH_2$ site is a minor channel through the whole temperature range studied.

The predicted total rate constants at 1 atm pressure are fitted by the modified three-parameter Arrhenius expressions in two different temperature ranges in order to reproduce the observed curvatures in their plots.

Acknowledgment. Chong-Wen Zhou thanks the Chinese Science Council for her Fellowship supporting her exchange visit to Florida International University. This work was also funded in part by the Chemical Sciences, Geosciences and Biosciences Division, Office of Basic Energy Sciences, Office of Sciences of the U.S. Department of Energy (Grant No. DE-FG02-04ER15570). X.Y.L. acknowledges the support received from National Natural Science Foundation of China (No. 20572073).

Supporting Information Available: Rotational constants I_i and vibrational frequencies of the species involved in the rate constants calculations computed at the BHandHLYP/6-311++G(d,p) level (Table S1), calculated energies obtained at the CCSD(T)//BHandHLYP/6-311++G(d,p) level for the reactions of OH with (*E*)-1-propenol (Table S2), (*Z*)-1-propenol (Table S3), and *syn*-propen-2-ol (Table S4). This information is available free of charge via the Internet at http://pubs.acs.org.

References and Notes

(1) Taatjes, C. A.; Hansen, N.; McIlroy, A.; Miller, J. A.; Senosiain, J. P.; Klippenstein, S. J.; Qi, F.; Sheng, L.; Zhang, Y.; Cool, T. A.; Wang, J.; Westmoreland, P. R.; Law, M. E.; Kasper, T.; Kohse-Höinghaus, K. *Science* **2005**, *308*, 1887.

(2) Erlenmeyer, E. *Chem. Ber.* **1880**, *13*, 305.

(3) Blank, B.; Fischer, H. *Helv. Chim. Acta* **1973**, *56*, 506.

(4) Saito, S. *Chem. Phys. Lett.* **1976**, *42*, 399.

(5) Cool, T. A.; Nakajima, K.; Mostefaoui, T. A.; Qi, F.; McIlroy, A.; Westmoreland, P. R.; Law, M. E.; Poisson, L.; Peterka, D. S.; Ahmed, M. *J. Chem. Phys.* **2003**, *119*, 8356.

(6) Taatjes, C. A.; Hansen, N.; Miller, J. A. *J. Phys. Chem. A* **2006**, *110*, 3254.

(7) Wang, J.; Li, Y. Y.; Zhang, T. C.; Tian, Z. Y.; Yang, B.; Zhang, K. W.; Qi, F.; Zhu, A. G.; Gui, Z. F.; Ng, C. Y. *Astrophys. J.* **2008**, *676*, 416.
(8) Zhou, C. W.; Li, Z. R.; Li, X. Y. *J. Phys. Chem.* **2009**, *113*, 2372.
(9) Zhou, C. W.; Li, Z. R.; Liu, C. X.; Li, X. Y. *J. Chem. Phys.* **2008**, *129*, 234301.
(10) Aloisio, S.; Francisco, J. S. *J. Phys. Chem. A* **2000**, *104*, 3211.
(11) Alvarez-Idaboy, J. R.; Mora-Diez, N.; Boyd, R. J.; Viver-Bunge, A. *J. Am. Chem. Soc.* **2001**, *123*, 2018.
(12) Alvarez-Idaboy, J. R.; Mora-Diez, N.; Viver-Bunge, A. *J. Am. Chem. Soc.* **2000**, *122*, 3715.
(13) Vasvári, V.; Szilágyi, I.; Bencsura, A.; Dóbe, S.; Berces, T.; Henon, E.; Canneaux, S.; Bohr, F. *Phys. Chem. Chem. Phys.* **2001**, *3*, 551.
(14) Yamada, T.; Taylor, P. H.; Goumri, A.; Marshall, P. *J. Chem. Phys.* **2003**, *119*, 10600.
(15) Galano, A. *J Phys. Chem. A* **2006**, *110*, 9153.
(16) Smith, I. W. M.; Ravishankara, A. R. *J. Phys. Chem. A* **2002**, *106*, 4798.
(17) Loomis, R. A.; Lester, M. I. *J. Chem. Phys.* **1995**, *103*, 4371.
(18) Lester, M. I.; Pond, B. V.; Anderson, D. T.; Harding, L. B.; Wagner, A. F. *J. Chem. Phys.* **2000**, *113*, 9889.
(19) Sekušak, S.; Sabljić, A. *Chem. Phys. Lett.* **1997**, *272*, 353.
(20) Robinson, P. J.; Holbrook, K. A. *Unimolecular Reaction*; Wiley-Interscience: London, 1972.
(21) Frisch, Æ.; Frisch, M. J.; Trucks, G. W. *Gaussian 03 User's Reference*. Gaussian Inc.: Pittsburgh, PA, 2003.
(22) Zhang, Q.; Bell, R.; Truong, T. N. *J. Phys. Chem.* **1995**, *99*, 592.
(23) Durant, J. L. *Chem. Phys. Lett.* **1996**, *256*, 595.
(24) Braïda, B.; Hiberty, P. C.; Savin, A. *J. Phys. Chem. A* **1998**, *102*, 7872.
(25) Sastry, G. N.; Bally, T.; Hrouda, V.; Cársky, P. *J. Am. Chem. Soc.* **1998**, *120*, 9323.
(26) Oxgaard, J.; Wiest, O. *J. Phys. Chem. A* **2001**, *105*, 8236.
(27) Rice, B. M.; Pai, S. V.; Chabalowski, C. F. *J. Phys. Chem. A* **1998**, *102*, 6950.
(28) Zhang, Y.; Zhao, C. Y.; You, X. Z. *J. Phys. Chem. A* **1997**, *101*, 2879.
(29) Gonzalez, C.; Schlegel, H. B. *J. Chem. Phys.* **1989**, *90*, 2154.
(30) Frisch, M. J.; Trucks, G. W.; Schlegel, H. B.; et al. *GAUSSIAN 03 B05*; Gaussian Inc.: Pittsburgh, 2003.
(31) Amos, R. D.; Bernhardsson, A.; Berning, A.; Celani, P.; Cooper, D. L.; Deegan, M. J. O.; Dobbyn, A. J. Eckert, F.; Hampel, C.; Hetzer, G.; Knowles, P. J.; Korona, T.; Lindh, R.; Lloyd, A. W.; McNicholas, S. J.; Manby, F. R.; Meyer, W.; Mura, M. E.; Nicklaβ, A.; Palmieri, P.; Pitzer, R.; Rauhut, G.; Schütz, M.; Schumann, U.; Stoll, H.; Stone, A. J. Tarroni, R.; Thorsteinsson, T.; Werner, H.-J. *MOLPRO version 2002.6*; University of Birmingham: Birmingham, U.K., 2003.
(32) Klippenstein, S. J.; Wagner, A. F.; Dunbar, R. C.; Wardlaw, D. M.; Robertson, S. H. *VariFlex, version 1.0*; Argonne National Laboratory: Argonne, IL, 1999.
(33) Gilbert, R. G.; Smith, S. C. *Theory of Unimolecular and Recombination Reactions*; Blackwell Scientific: Carlton, Australia, 1990.
(34) Holbrook, K. A.; Pilling, M. J.; Robertson, S. H. *Unimolecular Reactions*; Wiley: New York, 1996.
(35) Robertson, S. H.; Wagner, A. F.; Wardlaw, D. M. *Faraday Discuss. Chem. Soc.* **1995**, *102*, 65.
(36) Zhu, R. S.; Park, J.; Lin, M. C. *Chem. Phys. Lett.* **2005**, *408*, 25.
(37) Zhu, R. S.; Xu, Z. F.; Lin, M. C. *J. Chem. Phys.* **2004**, *120*, 6566.
(38) Sekušak, S.; Liedl, K. R.; Sabljić, A. *J. Phys. Chem. A* **1998**, *102*, 1583.
(39) Mourits, F. M.; Rummens, F. H. A. *Can. J. Chem.* **1977**, *55*, 3007.
(40) Zhu, R. S.; Lin, M. C. *ChemPhysChem.* **2004**, *5*, 1864.
(41) Lee, C.; Yang, W.; Parr, R. G. *Phys. Rev. B* **1998**, *37*, 785.
(42) Sansón, J. A.; Sánchez, M.-L.; Corchado, J. C. *J. Phys. Chem. A* **2006**, *110*, 589.
(43) Eckart, C. *Phys. Rev.* **1930**, *35*, 1303.
(44) Senosiain, J. P.; Klippenstein, S. J.; Miller, J. A. *J. Phys. Chem. A* **2006**, *110*, 6960.

JP903103S